Japanese Journal of Applied Physics

REGULAR PAPER

Spectroscopic estimation of the photon number for superconducting Kerr parametric oscillators

To cite this article: Keisuke Matsumoto *et al* 2023 *Jpn. J. Appl. Phys.* **62** SC1097

Japanese Journal of Applied Physics 62, SC1097 (2023) **REGULAR PAPER**
https://doi.org/10.35848/1347-4065/acc3a8

Spectroscopic estimation of the photon number for superconducting Kerr parametric oscillators

Keisuke Matsumoto[1,2*], Aiko Yamaguchi[3,4], Tsuyoshi Yamamoto[3,4], Shiro Kawabata[2,4], and Yuichiro Matsuzaki[2,4*]

[1]Department of Physics, Tokyo University of Science, 1-3, Kagurazaka, Shinjuku-ku, Tokyo 162-8601, Japan
[2]Research Center for Emerging Computing Technologies, National Institute of Advanced Industrial Science and Technology (AIST), Umezono1-1-1, Tsukuba, Ibaraki 305-8568, Japan
[3]Secure System Platform Research Laboratories, NEC Corporation, 1753, Shimonumabe, Kawasaki, Kanagawa 211-0011, Japan
[4]NEC-AIST Quantum Technology Cooperative Research Laboratory, National Institute of Advanced Industrial Science and Technology (AIST), Tsukuba, Ibaraki 305-8568, Japan

[*]E-mail: 1221544@ed.tus.ac.jp; matsumoto-kei@aist.go.jp; matsuzaki.yuichiro@aist.go.jp

Received February 28, 2023; revised March 6, 2023; accepted March 12, 2023; published online April 3, 2023

Quantum annealing (QA) is a way to solve combinational optimization problems. Kerr nonlinear parametric oscillators (KPOs) are promising devices for implementing QA. When we solve the combinational optimization problems using KPOs, it is necessary to precisely control the photon number of the KPOs. Here, we propose a feasible method to estimate the photon number of the KPO. We consider coupling an ancillary qubit to the KPO and show that spectroscopic measurements on the ancillary qubit provide information on the photon number of the KPO.

1. Introduction

Recently, much attention has been paid to Kerr nonlinear parametric oscillators (KPOs).[1–6] KPO is based on Kerr-nonlinear resonators driven by two-photon excitation,[7,8] which can be realized by using superconducting resonators.[9–11] It is known that the KPO can be used as a qubit for a gate-type quantum computer.[12–15] Recently, it has been shown that we can observe quantum phase transitions of the KPOs, which is useful for quantum metrology.[16–19]

Also, KPO is a promising candidate for realizing quantum annealing (QA).[1,20] QA is one of the techniques to solve combinational optimization problems.[21,22] The solution to the problems can be embedded into a ground state of the Ising Hamiltonian, and we can obtain the ground state of the Ising Hamiltonian after performing QA as long as the adiabatic condition is satisfied.[23]

Importantly, the Hamiltonian of the KPOs can be mapped into an Ising Hamiltonian.[1,20] To implement QA with KPOs, we start from vacuum states, and we gradually increase parametric driving terms in an adiabatic way. Then, the network of the KPOs finds a ground state of the Hamiltonian via a bifurcation process. A feasible architecture for QA with KPOs using nearest-neighbor interactions has also been proposed.[20,24] There are many applications of KPOs for QA.[25–27]

However, in order to accurately map the Ising Hamiltonian to the KPO Hamiltonian, we need to precisely control the average number of photons of each KPO. Although there is a formula to calculate the number of photons of the KPO under a semi-classical approximation, the calculated value can be different from the actual value.[28] So a reliable way to estimate the number of the photons of the KPO is required to solve practical combinational optimization problems.

In this paper, we propose a method to estimate the number of photons of the KPO from spectroscopic measurement. We consider a system, where the KPO is coupled with an ancillary qubit such as a superconducting transmon qubit with a frequency tunability[29,30] or another KPO (without parametric drive), as shown in Fig. 1. We couple a transmission line with the ancillary qubit. Driving the qubit through the transmission line, we can readout the information of the qubit by measuring reflected fields.[31,32] Alternatively, to measure the population of the transmon qubit, we can couple a resonator with the qubit for the dispersive readout.[33–35] We show that spectroscopic measurements on the ancillary qubit provide an estimate of the number of photons of the KPO. We evaluate the performance of our method with numerical simulations by solving a master equation and show that the proposed method is more accurate than the conventional method. It is worth mentioning that, in our previous study, by numerical methods, we investigate a case only when the driving strength is weak and the rotating wave approximation is valid.[36] On the other hand, in this paper, by using both numerical and analytical methods, we analyze the case with strong driving where the rotating wave approximation is violated. Moreover, in this paper, we study how the performance of our scheme changes with the detuning of the KPO. These results in this paper provide a deep understanding of our scheme to estimate the number of photons.

The paper is organized as follows. In Sect. 2, we introduce a model of a KPO coupled with an ancillary qubit. In Sect. 3, we describe our method to estimate the number of the photons of the KPO by spectroscopic measurements. In Sect. 4, we evaluate the performance of our method by using numerical simulations. In Sect. 5, we conclude our discussion. Throughout this paper, we set $\hbar = 1$.

2. Model Hamiltonian

In this section, we introduce a model of a KPO coupled with an ancillary qubit. The Hamiltonian is given by

$$\begin{aligned}\hat{H} = {}& \omega_{\mathrm{KPO}}\, \hat{a}^\dagger\hat{a} - \frac{\chi}{12}(\hat{a} + \hat{a}^\dagger)^4 \\ & + 2\beta(\hat{a} + \hat{a}^\dagger)^2 \cos\omega_{\mathrm{p}} t \\ & + \frac{\omega_{\mathrm{g}}}{2}\hat{\sigma}_z + g(\hat{a} + \hat{a}^\dagger)\hat{\sigma}_x + \lambda\hat{\sigma}_x \cos\omega_c t, \end{aligned} \tag{1}$$

where $\hat{a}^\dagger$ ($\hat{a}$) is a creation (annihilation) operator of the KPO, ω_{KPO} is the frequency of the KPO, χ is the Kerr

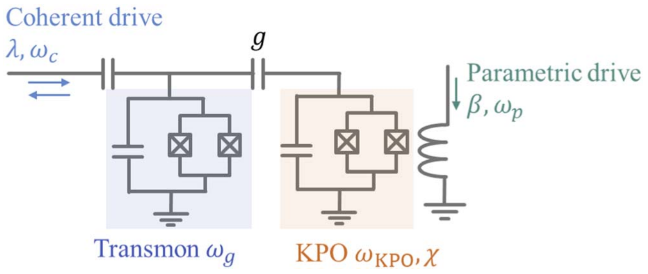

Fig. 1. (Color online) Schematic of a KPO coupled with a frequency-tunable transmon qubit. The transmon qubit is coupled to a transmission line. By driving the qubit through the transmission line and measuring the reflected fields, we can readout the information of the transmon qubit.

coefficient, β is the amplitude of a parametric drive, ω_p is the frequency of the parametric drive, ω_g is the frequency of the ancillary qubit, g is the coupling strength between the KPO and the ancillary qubit, and $\lambda(\omega_c)$ is the amplitude (frequency) of the driving field for the qubit, respectively. Here, $\hat{\sigma}_x$ and $\hat{\sigma}_z$ denote the Pauli operators. Moving into a rotating frame at the frequency of $\omega_\mathrm{p}/2$ and adapting the rotating wave approximation, the Hamiltonian is written as

$$\hat{H} = \hat{H}_{\mathrm{KPO}} + \hat{H}_{\mathrm{G}} + \hat{H}_{\mathrm{I}} + \hat{H}_{\mathrm{D}}, \tag{2}$$

$$\hat{H}_{\mathrm{KPO}} = \Delta\hat{a}^\dagger\hat{a} - \frac{\chi}{2}\hat{a}^\dagger\hat{a}^\dagger\hat{a}\hat{a} + \beta(\hat{a}^2 + \hat{a}^{\dagger 2}), \tag{3}$$

$$\hat{H}_{\mathrm{G}} = \frac{\omega_\mathrm{g} - \omega_\mathrm{p}/2}{2}\hat{\sigma}_z, \tag{4}$$

$$\hat{H}_{\mathrm{I}} = g(\hat{a}\hat{\sigma}_+ + \hat{a}^\dagger\hat{\sigma}_-), \tag{5}$$

$$\hat{H}_{\mathrm{D}} = \lambda_\mathrm{p}(\hat{\sigma}_+ e^{-i(\omega_c-\omega_\mathrm{p}/2)t} + \hat{\sigma}_- e^{i(\omega_c-\omega_\mathrm{p}/2)t}), \tag{6}$$

where $\Delta = \omega_{\mathrm{KPO}} - \chi - \omega_\mathrm{p}/2$ denotes the detuning of the KPO, $\lambda_\mathrm{p} = \lambda/2$ denotes the Rabi frequency of the ancillary qubit, and $\hat{\sigma}_\pm$ denotes the ladder operator. Throughout our paper, we set $\Delta < 0$. The ground and the first excited states of $\hat{H}_\mathrm{G}$ are $|\mathrm{g}\rangle$ and $|\mathrm{e}\rangle$, respectively. With $\beta = 0$, the Fock states $|n\rangle$ (for $n = 0, 1, 2, 3$) become eigenstates of the H_{KPO}. For $\beta \gg |\chi|$, on the other hand, the corresponding eigenstates are approximately given by $(|\alpha\rangle + |-\alpha\rangle)/\sqrt{2}$, $(|\alpha\rangle - |-\alpha\rangle)/\sqrt{2}$, $(D_\alpha + D_{-\alpha})|1\rangle/\sqrt{2}$, and $(D_\alpha - D_{-\alpha})|1\rangle/\sqrt{2}$, where $D_\alpha = \exp(\alpha\hat{a} - \alpha^*\hat{a}^\dagger)$ denotes a displacement operator.[1)]

When a linear resonator is coupled with a transmon qubit, we can realize a dispersive interaction described as $H'_\mathrm{I} = g\hat{\sigma}_z\hat{a}^\dagger\hat{a}$. In this case, we can measure the number of photons of the resonator by using the transmon qubit.[37–40)] However, to our best knowledge, there are no existing methods to realize the dispersive interaction between the transmon qubit and the KPO that is driven by the parametric drive. Moreover, $H'_\mathrm{I} = g\hat{\sigma}_z\hat{a}^\dagger\hat{a}$ does not commute with $\hat{H}_{\mathrm{KPO}}$, and it is known that such a non-commutable interaction is not suitable to readout the information of the target system.[41)] In principle, if we quickly turn off the parametric pump and non-linearity ($\beta = \chi = 0$), the KPO becomes the same as the linear resonator and we can realize the dispersive interaction when the frequency of the KPO is detuned from that of the transomon qubit. However, in this case, we need fast measurements, including pulse operations, which is much more difficult than our proposed method to require only continuous wave measurement.

3. Methods

In this section, we propose a method to estimate the number of photons of the KPO from a spectroscopic measurement of an ancillary qubit coupled with the KPO. As we explained, for sufficiently large β, the ground state of the KPO is approximately described by a superposition of two coherent states, namely $|\alpha\rangle$ and $|-\alpha\rangle$ where $\pm\alpha$ is the amplitude of the coherent state. Without loss of generality, we can assume that α is a real number. Then, the Hamiltonian of the ancillary qubit is approximately written as

$$\hat{H}^{\mathrm{eff}}_{\mathrm{qubit}} = \frac{\omega_\mathrm{g} - \omega_\mathrm{p}/2}{2}\hat{\sigma}_z \pm g\alpha\,\hat{\sigma}_x + \lambda_\mathrm{p}(\hat{\sigma}_+ e^{-i\Delta_\mathrm{q}t} + \hat{\sigma}_- e^{i\Delta_\mathrm{q}t}), \tag{7}$$

where $\Delta_\mathrm{q} = \omega_c - \omega_\mathrm{p}/2$ denotes a detuning of the coherent drive.[1)]

It is known that we can observe a Mollow triplet via a spectroscopic measurement with this Hamiltonian, where resonant transition frequencies are $\Delta_\mathrm{q} = 0,\ \pm 2g\alpha$.[42–47)] Since we can estimate the value of g from a separate spectroscopic measurement by observing a vacuum Rabi splitting,[48,49)] we can obtain the value of α from the peak (dip) positions observed in the Mollow triplet. It is worth mentioning that our method using the ancillary qubit may affect the dynamics of the KPO due to the resonant condition between the KPO and the ancillary qubit. This means that we may be unable to use our method to estimate the number of photons in the middle of computation. However, for QA and gate-type quantum computation, we can apply our method just before the readout at the end of the calculation. Alternatively, we can use our method to know the average number of photons before we start the computation. In these cases, during the computation, we can set the detuning between the KPO and the ancillary qubit so that the ancillary qubit should not affect the dynamics of the KPO. For this purpose, we could use a frequency tunable transmon qubit as an ancillary qubit.[29,30)] Therefore, our method is especially useful for QA and gate-type quantum computation.

With a conventional method,[14)] an analytical formula under semi-classical approximations such as $\alpha_{\mathrm{ana}} = \sqrt{(2\beta + \Delta)/\chi}$ is used to estimate the number of photons of the KPO when β is much larger than the decay rate γ_1. Importantly, previous research shows that the value of $\alpha_{\mathrm{ana}} = \sqrt{(2\beta + \Delta)/\chi}$ can provide a wrong estimate[28)] due to the violation of the approximation. Therefore, it is crucial to adopt more reliable method to estimate the number of photons especially when the conventional method provides an inaccurate estimation.

4. Numerical simulations

In this section, we evaluate the performance of our method by comparing with the conventional method using numerical simulations of the Gorini–Kossakowski–Sudarshan–Lindblad (GKSL) master equation. Here, we adopt the Hamiltonian in Eq. (2). To take the effect of photon loss into account, we use the following GKSL master equation

$$\frac{\partial \rho}{\partial t} = -i[\hat{H}_{\mathrm{KPO}} + \hat{H}_{\mathrm{G}} + \hat{H}_{\mathrm{I}} + \hat{H}_{\mathrm{D}}, \rho] + \frac{\gamma_1}{2}(2\hat{a}\rho\hat{a}^{\dagger} - \{\hat{a}^{\dagger}\hat{a}, \rho\}) + \frac{\gamma_2}{2}(2\hat{\sigma}_{-}\rho\hat{\sigma}_{+} - \{\hat{\sigma}_{+}\hat{\sigma}_{-}, \rho\}), \quad (8)$$

where γ_1 denotes the one photon dissipation rate of the KPO, γ_2 denotes the spontaneous emission rate of the ancillary qubit, and $\hat{\rho}$ denotes the density matrix describing the quantum state of the total system. We solve the GKSL master equation Eq. (8) using QuTiP.[50] We choose the initial state as a steady state of Eq. (8) with $\lambda_{\mathrm{p}} = 0$. Also, we set $\omega_g = \omega_{\mathrm{p}}/2$.

In Fig. 2(a), we plot a time-integrated spectra $I = (1/t)\int_0^t d\tau\ (\langle\hat{\sigma}_z\rangle + 1)/2$ as a function of Δ_{q} with a step of 0.05 MHz, where $\langle\hat{\sigma}_z\rangle = \mathrm{Tr}[\hat{\sigma}_z\rho]$, which is effectively the same as a spectroscopy to detect the change in the population of the qubit.

This spectra is upper (lower) bounded by 1 (0). The value of this spectra depends on the Rabi frequency and decay rate of the qubit. The observed peak and dips are at $\Delta_{\mathrm{q}}^{(0)}/2\pi = 1.35$ MHz, $\Delta_{\mathrm{q}}^{(1)}/2\pi = -16.80$ MHz and $\Delta_{\mathrm{q}}^{(2)}/2\pi = 17.10$ MHz, respectively.

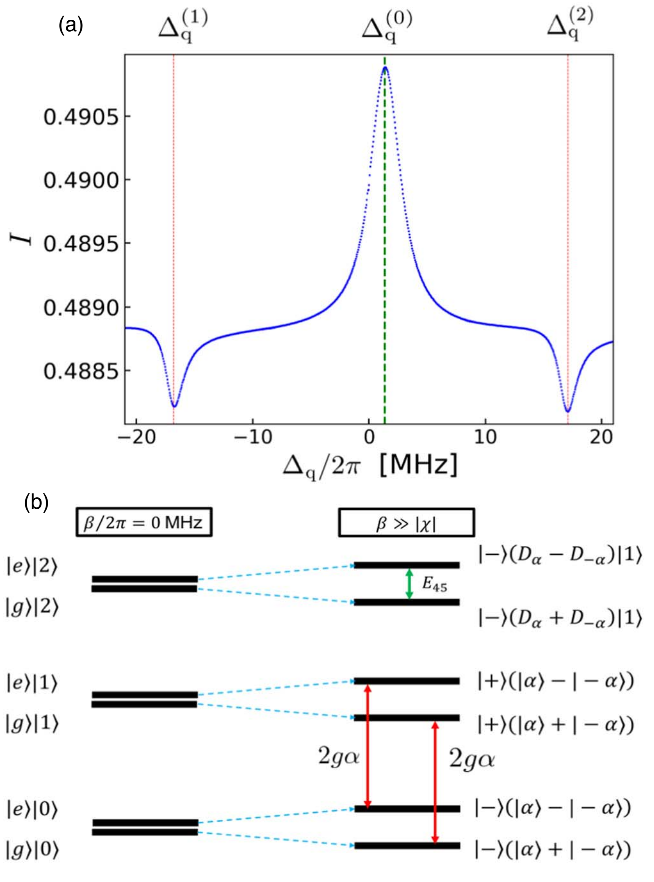

Fig. 2. (Color online) (a) The time-integrated spectra I against $\Delta_{\mathrm{q}}/2\pi$ with $\lambda_{\mathrm{p}}/2\pi = 0.5$ MHz. We set the parameters as $\Delta/2\pi = -30.0$ MHz, $\chi/2\pi = 18.0$ MHz, $\beta/2\pi = 42.0$ MHz, $g/2\pi = 5.0$ MHz, $\gamma_1/2\pi = \gamma_2/2\pi = 0.8$ MHz, and $\omega_g = \omega_{\mathrm{p}}/2$. (b) The energy diagram of the states of a KPO coupled with a qubit. In the left (right) side, we show the energy diagram with $\beta/2\pi = 0$ MHz ($\beta \gg |\chi|$). Here, $|\alpha\rangle$ and $|n\rangle$ (for $n = 0$, 1, 2) denote a coherent state and Fock states, respectively, while $D_\alpha = \exp(\alpha\hat{a} - \alpha^{*}\hat{a}^{\dagger})$ denotes the discplacement operator. Also, $|g\rangle$ ($|e\rangle$) and $|\pm\rangle = \frac{1}{\sqrt{2}}(|g\rangle \pm |e\rangle)$ denotes the ground (excited) state and the superposition states of the qubit.

Figure 2(b) shows the energy diagram composed of the system of the KPO coupled with an ancillary qubit. We calculate the energy eigenvalues of the Hamiltonian, and we confirm that the energy difference between the eigenvalues is almost the same as the peak frequency observed in our numerical simulation. The dip at $\Delta_{\mathrm{q}}^{(1)}/2\pi = -16.80$ MHz ($\Delta_{\mathrm{q}}^{(2)}/2\pi = 17.10$ MHz) corresponds to the transition between the ground (first excited) state and the second (third) excited state, which we describe by a red vertical arrow in Fig. 2(b). Here, with our parameters, the ground state, first excited state, second excited state, and third excited state are approximately described as $|-\rangle(|\alpha\rangle + |-\alpha\rangle)$, $|-\rangle(|\alpha\rangle - |-\alpha\rangle)$, $|+\rangle(|\alpha\rangle + |-\alpha\rangle)$, and $|+\rangle(|\alpha\rangle - |-\alpha\rangle)$, respectively. On the other hand, the peak at $\Delta_{\mathrm{q}}^{(0)}/2\pi = 1.35$ MHz corresponds to a transition between the fourth excited state and the fifth excited state, which we describe by a green vertical arrow in Fig. 2(b), where the fourth (fifth) excited state is approximately given as $|-\rangle(\hat{D}_\alpha + \hat{D}_{-\alpha})|2\rangle$ ($|-\rangle(\hat{D}_\alpha - \hat{D}_{-\alpha})|2\rangle$). Actually, from the numerical simulation, the population of the fourth (fifth) excited state at $t = 0$ is 0.005 90 (0.0173) and becomes finally 0.007 72 (0.0155) at $t = 3\ \mu$s. This means that the coherent drive actually induces a transition between the fourth excited state and the fifth excited state. By diagonalizing the Hamiltonian, we recognized that we have a transition between the second excited state and the third excited state with an energy difference of $2\pi \times 0.5$ MHz. However, we cannot resolve this peak in the numerical simulation possibly due to the large width of the peak at $\Delta_{\mathrm{q}}^{(0)}$.

Now, let us discuss the estimation of the number of photons. We consider a steady state $\hat{\rho}_{\mathrm{ss}}$ of Eq. (8) with $\lambda_{\mathrm{p}} = 0$ and $g = 0$, and we define $\mathrm{Tr}[\rho_{\mathrm{ss}}\hat{a}^{\dagger}\hat{a}] = |\alpha|^2$. Let us define a relative error of $|\alpha|^2$ estimated by using our method as $\epsilon_1 \equiv ||\alpha_{\mathrm{est}}|^2 - |\alpha|^2|/|\alpha|^2$, where $|\alpha|^2(|\alpha_{\mathrm{est}}|^2)$ is the actual (estimated) value of the photon number of the KPO. Also, when we use the analytical formula, the relative error of the estimated $|\alpha|^2$ is defined as $\epsilon_2 \equiv ||\alpha_{\mathrm{anal}}|^2 - |\alpha|^2|/|\alpha|^2$.

From Fig. 2(a), we observe two dips at $\Delta_{\mathrm{q}}^{(1)}$ and $\Delta_{\mathrm{q}}^{(2)}$ and the frequency difference is $(\Delta_{\mathrm{q}}^{(2)} - \Delta_{\mathrm{q}}^{(1)})/2\pi = 33.90$ MHz. We can estimate the number of photons from this, as we explained before. Since we set $g/2\pi = 5$ MHz, we obtain an estimated value of $|\alpha_{\mathrm{est}}|^2 = 2.87$, where we solve an equation of $4g\alpha_{\mathrm{est}}/2\pi = (\Delta_{\mathrm{q}}^{(2)} - \Delta_{\mathrm{q}}^{(1)})/2\pi = 33.90$ MHz. The relative error is calculated as $\epsilon_1 = 0.0280$. On the other hand, when we use the analytical formula, we obtain $\epsilon_2 = 0.0672$. This result indicates that our method provides a more accurate estimate of α than the conventional method.

Also, to further quantify the performance of our method, we calculate the relative error of our methods with other parameters, and compare the error with that of the conventional method. When the detuning is too large for the KPO to bifurcate, the ground state of the KPO is not the superposition of the coherent states anymore. Thus, when we plot Figs. 3 and 4, we choose a range of detuning for the KPO to bifurcate in these numerical simulations.

In Fig. 3, we plot the relative error against the detuning of the KPO Δ. In Fig. 4, we plot the relative error against Δ by setting β to satisfy a condition of $(2\beta + \Delta)/2\pi = 50$ MHz. The reason why we choose this condition is that the estimated photon number $|\alpha_{\mathrm{anal}}|^2$ from the analytical formula is fixed in these numerical simulations. From Figs. 3 and 4, our method

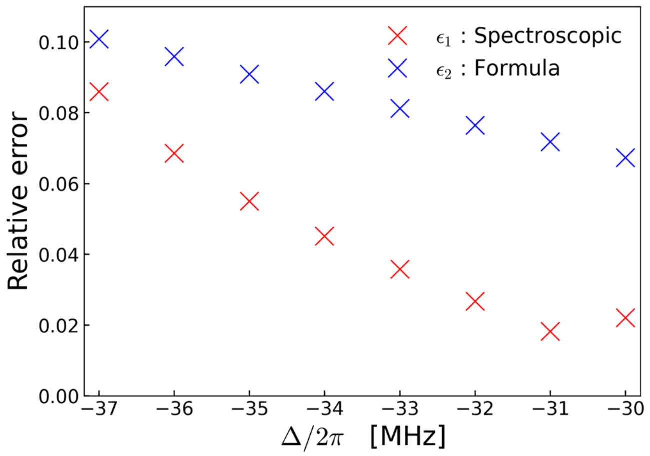

Fig. 3. (Color online) Plot of the relative error $||\alpha_{est}|^2 - |\alpha|^2|/|\alpha|^2$ against the detuning of the KPO where $|\alpha|^2$ ($|\alpha_{est}|^2$) is the true (estimated) value of the photon number. We set the parameters as $\chi/2\pi = 18.0$ MHz, $\beta/2\pi = 42.0$ MHz, $g/2\pi = 5.0$ MHz, $\lambda_p/2\pi = 0.5$ MHz, $\gamma_1/2\pi = \gamma_2/2\pi = 0.8$ MHz, and $\omega_g = \omega_p/2$.

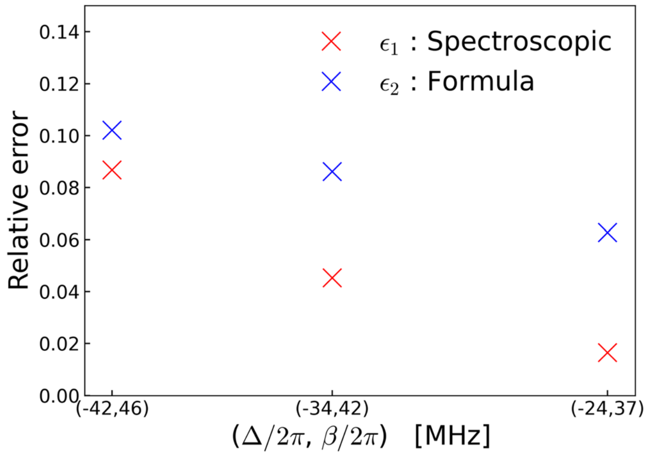

Fig. 4. (Color online) Plot of the relative error $||\alpha_{est}|^2 - |\alpha|^2|/|\alpha|^2$ against the detuning of the KPO where $|\alpha|^2$ ($|\alpha_{est}|^2$) is the true (estimated) value of the photon number. We set β to satisfy a condition of $(2\beta + \Delta)/2\pi = 50$ MHz. Also, we set the parameters as $\chi/2\pi = 18.0$ MHz, $g/2\pi = 5.0$ MHz, $\lambda_p/2\pi = 0.5$ MHz, $\gamma_1/2\pi = \gamma_2/2\pi = 0.8$ MHz, and $\omega_g = \omega_p/2$.

provides a more accurate estimate of $|\alpha|^2$ than the conventional method when there is a detuning Δ. Figure 3 shows a non-monotonic dependence of the relative error on the detuning. Thus, we find that there is an optimal detuning to minimize the relative error for our method. It is worth mentioning that, in the original proposal of QA with KPO,[1)] KPO has a finite detuning during QA. Therefore, our scheme is useful for such circumstances.

Furthermore, we investigate how a stronger Rabi frequency affects spectroscopic measurements. We perform numerical simulations with a Rabi frequency of $\lambda/2\pi = 2$ MHz. It is worth mentioning that we observe not only the prominent two dips but also small dips at $\Delta_q^{(3)}/2\pi = -8.40$ MHz and $\Delta_q^{(4)}/2\pi = 8.65$ MHz, in Fig. 5. We expect that these additional dips come from the violation of the rotating wave approximation, which will be discussed in the Appendix.

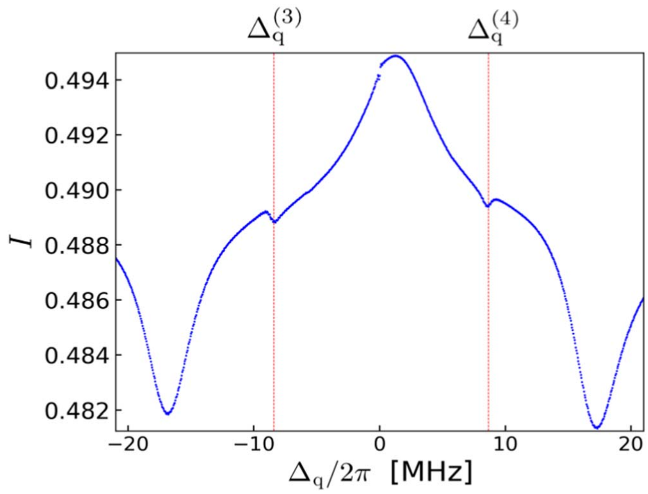

Fig. 5. (Color online) (a) The time-integrated spectra I against the detuning $\Delta_q/2\pi$ with the Rabi frequency $\lambda_p/2\pi = 2$ MHz. We use the same parameters as those in Fig. 2(a) except the Rabi frequency. We observe not only the main two dips but also small dips at $\Delta_q^{(3)}/2\pi = -8.40$ MHz and $\Delta_q^{(4)}/2\pi = -8.65$ MHz.

Let us remark that, although the ground state of the KPO is a superposition of two coherent states, we have a classical mixture of two coherent states in our numerical simulations due to the photon loss. Similarly, if we perform QA with a problem Hamiltonian whose ground states are degenerate, we will obtain not the superposition of the ground states but the classical mixture between them. Fortunately, this does not affect the performance of QA for the following reason. When we solve combinational optimization problems with QA, the purpose is not to obtain all degenerate ground states but to obtain one of the ground state. So, even if the state after QA is a classical mixture of the degenerate ground states, single shot measurements of KPOs project the states into one of the ground states, and we obtain the answer.

5. Conclusion

In conclusion, we propose an experimentally feasible method to estimate the number of photons of the KPO. We couple an ancillary qubit with the KPO, and spectroscopic measurements of the qubit let us know the number of photons of the KPO. Our results are essential to realize QA with KPOs for solving combinational optimization problems.

This work was supported by MEXTs Leading Initiative for Excellent Young Researchers, JST PRESTO (Grant No. JPMJPR1919), Japan. This paper is partly based on the results obtained from a project, JPNP16007, commissioned by the New Energy and Industrial Technology Development Organization (NEDO), Japan.

Appendix. Calculation of the transition frequencies by using the perturbation theory

In this appendix, to understand the violation of the rotating wave approximation in Fig. 5, we calculate the second-order of the transition probability with the effective qubit Hamiltonian Eq. (7). We consider the following Hamiltonian

$$\hat{H} = g\alpha\ \hat{\sigma}_x + \lambda_p(\hat{\sigma}_+ e^{-i\Delta_q t} + \hat{\sigma}_- e^{i\Delta_q t}). \qquad \text{(A·1)}$$

We can rewrite this Hamiltonian as

$$\hat{H} = g\alpha\hat{\sigma}_x + \frac{\lambda_p}{2}[(\hat{\sigma}_x + i\hat{\sigma}_y)e^{-i\Delta_q t} + (\hat{\sigma}_x - i\hat{\sigma}_y)e^{i\Delta_q t}], \tag{A·2}$$

where we use $\hat{\sigma}_{\pm} = (\hat{\sigma}_x \pm i\hat{\sigma}_y)/2$. We change the notation from $\{\hat{\sigma}_x, \hat{\sigma}_y, \hat{\sigma}_z\}$ to $\{\hat{Z}, \hat{Y}, \hat{X}\}$, and get

$$\hat{H} = g\alpha\ \hat{Z} + \frac{\lambda_p}{2}[(\hat{Z} + i\hat{Y})e^{-i\Delta_q t} + (\hat{Z} - i\hat{Y})e^{i\Delta_q t}]. \tag{A·3}$$

We can rewrite the Hamiltonian as

$$\hat{H} = g\alpha\ \hat{Z} + \frac{\lambda_p}{2}\left(\left\{\hat{Z} + i\frac{\hat{\sigma}'_+ - \hat{\sigma}'_-}{i}\right\}e^{-i\Delta_q t} + \left\{\hat{Z} - i\frac{\hat{\sigma}'_+ - \hat{\sigma}'_-}{i}\right\}e^{i\Delta_q t}\right), \tag{A·4}$$

where we use $\hat{X} = \hat{\sigma}'_+ + \hat{\sigma}'_-$, $\hat{Y} = -i(\hat{\sigma}'_+ - \hat{\sigma}'_-)$. We move to an interaction picture defined by a unitary operation of $\hat{U} = \exp(i\ g\alpha\ \hat{Z})$. The Hamiltonian in this frame is written as

$$\hat{H}_I(t) = \frac{1}{2}(\hat{Z}e^{-i\Delta_q t} + \hat{\sigma}'_+ e^{i(2g\alpha - \Delta_q)t} - \hat{\sigma}'_- e^{-i(2g\alpha + \Delta_q)t} + \hat{Z}e^{i\Delta_q t} - \hat{\sigma}'_+ e^{i(2g\alpha + \Delta_q)t} + \hat{\sigma}'_- e^{i(-2g\alpha + \Delta_q)t}). \tag{A·5}$$

We solve a time-dependent Schrödinger equation in the interaction picture as

$$i\frac{d}{dt}|\psi(t)\rangle = \lambda_p \hat{H}_I(t)|\psi(t)\rangle. \tag{A·6}$$

By performing a perturbative expansion up to the second order, we obtain

$$|\psi(t)\rangle \simeq |\psi(0)\rangle + \lambda_p D_1|\psi(0)\rangle + \lambda_p^2 D_2|\psi(0)\rangle, \tag{A·7}$$

$$D_1 \equiv -i\int_0^t \hat{H}_I(t_1), \tag{A·8}$$

$$D_2 \equiv (-i)^2\int_0^t\int_0^{t_1} dt_2 \hat{H}_I(t_1)\hat{H}_I(t_2), \tag{A·9}$$

We calculate a transition probability from the initial state $|\psi(0)\rangle = |\psi_0\rangle$ to the final state $|\psi_f\rangle$ as follows.

$$|\langle\psi_f|\psi(t)\rangle|^2 \simeq |\langle\psi_f|\psi_0\rangle + C^{(1)}(t) + C^{(2)}(t)|^2, \tag{A·10}$$

$$C^{(1)}(t) = \lambda_p\langle\psi_f|D_1|\psi_0\rangle, \tag{A·11}$$

$$C^{(2)}(t) = \lambda_p^2\langle\psi_f|D_2|\psi_0\rangle. \tag{A·12}$$

In the limit of large (small) $\lambda_p(t)$ by fixing a value of $\lambda_p t$, we can calculate the first (second) order transition probability $|C^{(1)}|^2$ ($|C^{(2)}|^2$), and obtain as the following

$$|\langle\psi_f|\psi(t)\rangle|^2 \simeq |\langle\psi_f|\psi_0\rangle|^2 + A_1\ \delta(\Delta_q) + A_2\ \delta(2g\alpha + \Delta_q) + A_3\ \delta(2g\alpha - \Delta_q), \tag{A·13}$$

$$+A_4\ \delta(g\alpha + \Delta_q) + A_5\ \delta(g\alpha - \Delta_q), \tag{A·14}$$

where A_i (B_i) ($i = 1, 2, 3, 4, 5$) denotes coefficient determined by λ_p, g, α, and Δ_q. This result clarifies the origin of the dips observed at $\Delta_q^{(3)}$ and $\Delta_q^{(4)}$ in Fig. 5.

1) H. Goto, Sci. Rep. **6**, 1 (2016).
2) H. Goto, J. Phys. Soc. Jpn. **88**, 061015 (2019).
3) H. Goto, Z. Lin, T. Yamamoto, and Y. Nakamura, Phys. Rev. A **99**, 023838 (2019).
4) Z. Wang, M. Pechal, E. A. Wollack, P. Arrangoiz-Arriola, M. Gao, N. R. Lee, and A. H. Safavi-Naeini, Phys. Rev. X **9**, 021049 (2019).
5) A. Grimm, N. E. Frattini, S. Puri, S. O. Mundhada, S. Touzard, M. Mirrahimi, S. M. Girvin, S. Shankar, and M. H. Devoret, Nature **584**, 205 (2020).
6) T. Yamaji, S. Kagami, A. Yamaguchi, T. Satoh, K. Koshino, H. Goto, Z. Lin, Y. Nakamura, and T. Yamamoto, Phys. Rev. A **105**, 023519 (2022).
7) G. J. Milburn and C. A. Holmes, Phys. Rev. A **44**, 4704 (1991).
8) B. Wielinga and G. J. Milburn, Phys. Rev. A **48**, 2494 (1993).
9) J. Bourassa, F. Beaudoin, J. M. Gambetta, and A. Blais, Phys. Rev. A **86**, 013814 (2012).
10) C. H. Meaney, H. Nha, T. Duty, and G. J. Milburn, EPJ Quantum Technol. **1**, 7 (2014).
11) Z. Leghtas et al., Science **347**, 853 (2015).
12) P. T. Cochrane, G. J. Milburn, and W. J. Munro, Phys. Rev. A **59**, 2631 (1999).
13) H. Goto, Phys. Rev. A **93**, 050301(R) (2016).
14) S. Puri, S. Boutin, and A. Blais, npj Quantum Inf. **3**, 18 (2017).
15) S. Puri et al., Sci. Adv. **6**, eaay5901 (2020).
16) N. Bartolo, F. Minganti, W. Casteels, and C. Ciuti, Phys. Rev. A **94**, 033841 (2016).
17) F. Minganti, A. Biella, N. Bartolo, and C. Ciuti, Phys. Rev. A **98**, 042118 (2018).
18) M. Dykman, C. Bruder, N. Lörch, and Y. Zhang, Phys. Rev. B **98**, 195444 (2018).
19) R. Rota, F. Minganti, C. Ciuti, and V. Savona, Phys. Rev. Lett. **122**, 110405 (2019).
20) S. Puri, C. K. Andersen, A. L. Grimsmo, and A. Blais, Nat. Commun. **8**, 15785 (2017).
21) T. Kadowaki and H. Nishimori, Phys. Rev. E **58**, 5355 (1998).
22) E. Farhi, J. Goldstone, S. Gutmann, J. Lapan, A. Lundgren, and D. Preda, Science **292**, 472 (2001).
23) S. Morita and H. Nishimori, J. Math. Phys. (N.Y.) **49**, 125210 (2008).
24) W. Lechner, P. Hauke, and P. Zoller, Sci. Adv. **1**, e1500838 (2015).
25) S. E. Nigg, N. Lörch, and R. P. Tiwari, Sci. Adv. **3**, e1602273 (2017).
26) T. Onodera, E. Ng, and P. L. McMahon, npj Quantum Inf. **6**, 48 (2020).
27) H. Goto and T. Kanao, Commun. Phys. **3**, 235 (2020).
28) T. Kanao and H. Goto, npj Quantum Inf. **7**, 18 (2021).
29) J. Koch, T. M. Yu, J. Gambetta, A. A. Houck, D. I. Schuster, J. Majer, A. Blais, M. H. Devoret, S. M. Girvin, and R. J. Schoelkopf, Phys. Rev. A **76**, 042319 (2007).
30) R. Barends et al., Phys. Rev. Lett. **111**, 080502 (2013).
31) O. Astafiev, A. M. Zagoskin, A. Abdumalikov Jr, Y. A. Pashkin, T. Yamamoto, K. Inomata, Y. Nakamura, and J. S. Tsai, Science **327**, 840 (2010).
32) S. Masuda, A. Yamaguchi, T. Yamaji, T. Yamamoto, T. Ishikawa, Y. Matsuzaki, and S. Kawabata, New J. Phys. **23**, 093023 (2021).
33) F. Mallet, F. R. Ong, A. Palacios-Laloy, F. Nguyen, P. Bertet, D. Vion, and D. Esteve, Nat. Phys. **5**, 791 (2009).
34) T. Walter et al., Phys. Rev. Appl. **7**, 054020 (2017).
35) R. Vijay, D. Slichter, and I. Siddiqi, Phys. Rev. Lett. **106**, 110502 (2011).
36) K. Matsumoto, A. Yamaguchi, T. Yamamoto, S. Kawabata, and Y. Matsuzaki, Ext. Abstr. Solid State Devices and Materials, 2022, p. 187.
37) B. Johnson et al., Nat. Phys. **6**, 663 (2010).
38) R. Dassonneville, R. Assouly, T. Peronnin, P. Rouchon, and B. Huard, Phys. Rev. Appl. **14**, 044022 (2020).
39) A. Essig, Q. Ficheux, T. Peronnin, N. Cottet, R. Lescanne, A. Sarlette, P. Rouchon, Z. Leghtas, and B. Huard, Phys. Rev. X **11**, 031045 (2021).
40) J. C. Curtis, C. T. Hann, S. S. Elder, C. S. Wang, L. Frunzio, L. Jiang, and R. J. Schoelkopf, Phys. Rev. A **103**, 023705 (2021).
41) S. Endo, Y. Matsuzaki, K. Kakuyanagi, S. Saito, N. Lambert, and F. Nori, Sci. Rep. **10**, 1 (2020).
42) B. R. Mollow, Phys. Rev. **188**, 1969 (1969).

43) Q. Wu, D. J. Gauthier, and T. Mossberg, Phys. Rev. A **49**, R1519 (1994).
44) G. Wrigge, I. Gerhardt, J. Hwang, G. Zumofen, and V. Sandoghdar, Nat. Phys. **4**, 60 (2008).
45) A. Ulhaq, S. Weiler, S. M. Ulrich, R. Roßbach, M. Jetter, and P. Michler, Nat. Photonics **6**, 238 (2012).
46) X. Xu, B. Sun, P. R. Berman, D. G. Steel, A. S. Bracker, D. Gammon, and L. J. Sham, Science **317**, 929 (2007).
47) A. Laucht et al., Nat. Nanotechnol. **12**, 61 (2017).
48) A. Wallraff, D. I. Schuster, A. Blais, L. Frunzio, R. S. Huang, J. Majer, S. Kumar, S. M. Girvin, and R. J. Schoelkopf, Nature **431**, 162 (2004).
49) I. Chiorescu, P. Bertet, K. Semba, Y. Nakamura, C. Harmans, and J. Mooij, Nature **431**, 159 (2004).
50) J. R. Johansson, P. D. Nation, and F. Nori, Comput. Phys. Commun. **183**, 1760 (2012).

